AIAA SciTech Forum
12-16 January 2026, Orlando, FL
AIAA SCITECH 2026 Forum

10.2514/6.2026-2291

Efforts Towards Shear Stress and Heat Flux Measurement On a Hollow Cylinder at Mach 6

B. A. Segall*, T. C. Keenoy†, and N. J. Parziale‡
Stevens Institute of Technology, Hoboken, NJ 07030, USA

Shear stress and heat-flux surface quantities were measured on a fully-turbulent hollow cylinder at Mach 6 using shear stress sensors and temperature gauges. Experiments were conducted at the Stevens Shock Tunnel (SST) with a 'flight-enthalpy-matched' and a 'cold-flow' condition. Heat flux was recovered from temperature gradients using both the Cook-Felderman 1-D semi-infinite heat flux equation and an inverse FFT solution using Green's function. Temperature gauges were capable of recording µs level effects in the flow. Non-dimensionalising the recovered heat flux to Stanton Number vs Reynolds number shows 50% undershoot to the value theorized by correlations for turbulent flow conditions. In the future, the method of Whalen et al. [1] will be used to correct for errors associated with the sensing element being of finite depth. Wall shear sensor signal only exceeded the noise floor for the enthalpy-matched condition. Both measurements were non-dimensionalized to Stanton number and compared to correlations well documented in literature.

I. Introduction

Experimental validation of existing skin friction and heat flux correlations is vital for accurate predictions of aerodynamic drag and heat transfer to solid bodies in hypersonic flows [2]. A comprehensive understanding of these quantities is required for the design of modern hypersonic vehicles [3]. Wall heat flux measurements in reflected shock facilities like the Stevens Shock Tunnel are often made according to 1-D semi-infinite solid simplifications due to short test durations. A range of measurement techniques following this assumption have been evaluated [4]. The means of measuring heat flux on this time-scale include temperature sensitive paints (TSP) [5, 6], thin film sensors [7–9], and coaxial thermocouples [10, 11]. Temperature sensitive paint is relatively easy to experiment as the only materials needed are a coat or a substrate film of paint, a light source for thermal quenching and a high-speed camera. However, paint that has both a response of greater than 1 kHz and sensitivities of ± 0.1 K is both expensive and easily degraded. Models would need to be coated multiple times during a campaign to avoid paint photo-degradation. Thin film gauges and coaxial thermocouples are the state-of-the-art in current surface measurement techniques. Discrete sensors such as coaxial thermocouples and thin film arrays with small surface areas benefit from high frequency response to capture transient flow physics. Facilities such as CUBRC instrument numerous in-house thin film sensors to their models, citing the sensor's small sensing element size and insulating substrate as factors that make them ideal for resolving spatial and temporal heat transfer of test article surfaces [9]. CUBRC also used off-the-shelf Type-E coaxial thermocouples from Medtherm Corporation as these thermocouples are specialized in measuring surface temperature changes on hypersonic ground test articles. The thermocouples suffer from lower signal-to-noise ratio (SNR) at low heat transfer rates but are robust and durable for numerous test campaigns without maintenance.

Measurements in wall shear stress are also highly coveted by the hypersonic community. Recent advancements by Ahmic Aerospace in coaxial shear stress gauge construction have reduced senor uncertainty by means of sensor misalignment and pressure driven moments on the sensing element[12, 13]. These sensors function using an embedded cantilevered beam positioned flush with the test article to capture only shear forces along the article wall. Strain gauges at the base of the beam capture the deflection as flow passes over a floating element attached to the top of the beam. As with temperature measurements, the sensor time response and minimum fluid flow to exceed the noise floor must be known to understand ground test capabilities. Ahmic wall shear stress gauges have been successfully tested for flows with shear stress values in the range of 1-340 Pa with reported skin friction uncertainties of less that 10%. The working frequency of these sensors is on the scale of seconds and have been used primarily for blow down and in flight testing. Therefore, it is an open question of whether these gauges will capture transient phenomena within a <10 ms test window.

*Graduate Student, Mechanical Engineering, Castle Point on Hudson, Hoboken, New Jersey, 07030.
†Graduate Student, Mechanical Engineering, Castle Point on Hudson, Hoboken, New Jersey, 07030.
‡George Meade Bond Professor, Mechanical Engineering, Castle Point on Hudson, Hoboken, New Jersey, 07030, AIAA Associate Fellow.

This paper discusses the instrumentation of a hollow cylinder with coaxial heat flux and shear stress gauges, both supplied by Ahmic Aerospace. These components were instrumented at multiple locations along the test article to capture data in fully turbulent regions of hypersonic flow. This paper also serves as the shakedown of the capabilities of these sensors in the Stevens Shock Tunnel (SST) facility. Additionally, sensor data from this experiment campaign is compared to measured quantities from previous published krypton tagging velocimetry campaigns with efforts to validate skin friction and heat transfer correlations [14].

II. Experimental Setup

A. Ground-Test Facility and Run Conditions

Experiments were performed in the Stevens Shock Tunnel, which is a reflected-shock tunnel designed to duplicate Mach 6 flight, with matching enthalpy, Mach, and Reynolds number at 20 km [14–17]. The nozzle exit diameter is 16 inches (406 mm) and the test rhombus is approximately 13 inches (330 mm) high by 5 ft (1.5 m) long. The Mach 6 'enthalpy-matched' condition has a test time of 5 ms at unit Reynolds number up to 8×10^6 1/m and is executed with a He driver. For the 'cold-flow' condition, a N_2 driver was used, providing a longer 15 ms test time and an increased Reynolds number of up to 32×10^6 1/m (a 14×10^6 1/m and 16×10^6 1/m condition is used for this work). This reduces the reservoir enthalpy but provides sufficient heating such that the flow in the freestream does not condense. For this campaign, the test gas was N_2.Freestream conditions are calculated with Cantera [18] and the Shock and Detonation Toolbox [19] following the methods in Korte et al. [20] and Segall et al. [16]. The run conditions for this experiment can be found in Table 1

Table 1 SST Run Conditions for the 'cold flow' and 'enthalpy matched' conditions, where P_4 is driver-section nitrogen gas pressure; P_4/P_1 is the driver-to-driven pressure ratio that determines the driven air gas pressure P_1; u_s is the shock speed; M_s is the shock Mach number; T_R is the reservoir temperature; P_R is the reservoir pressure; P_∞ is the freestream pressure, T_∞ is the freestream temperature, M_∞ is the freestream Mach number, U_∞ is the time-averaged freestream velocity, and Re^u_∞ is the unit Reynolds number.

Shot	P_4 (MPa)	$\frac{P_4}{P_1}$	u_s (m/s)	M_s	P_R (MPa)	T_R (K)	P_∞ (kPa)	T_∞ (K)	M_∞	U_∞ (m/s)	Re^u_∞ (10^6 1/m)
Shot 518	3.44	10	545	1.53	2.07	520	1.18	66	6.25	980	12.3
Shot 521	7.58	117	1240	3.51	5.40	1696	3.16	232	5.91	1836	5.6

The test article is a hollow-cylinder flare (HCF) that fits within the inviscid test rhombus. This article featured in previous test campaigns including KTV and FLDI. The HCF is 1 m-long with a 0.102 m (4 in) outer diameter hollow cylinder and a 34° flare of maximum diameter 0.203 m (8 in). Three 40-grit sanding belt trips were placed on the test article to induce turbulence with distributed roughness: (1) 0.076 m (3 in) long at 0.026 m (1 in) from the sharp leading edge; (2) 0.076 m (3 in) long at 0.137 m (5.375 in); and (3) 0.222 m (8.75 in) long at 0.267 m (10.5 inches). The boundary layer is assumed to be in an equilibrium, turbulent state as supported by focused laser differential interferometry (FLDI) measurements reported in [14, 21]. The FLDI measurements were made upstream of the KTV measurements at 0.7 m (27.6 in) or $Re_x = 8.10 \times 10^6$ and $Re_x = 3.08 \times 10^6$ from the HCF leading edge for the cold-flow and enthalpy-matched conditions, respectively. Those results match those of DNS, bringing confidence to the understanding of the state of the boundary layer uniformity.

B. Instrumentation of the HC with shear stress and heat flux sensors

The HCF test article was instrumented with seven unsteady surface temperature gauges and two wall shear sensors, all supplied by Ahmic Aerospace. The locations of the upgraded instrumentation can be seen in Fig. 2. The locations on the cylinder and the Reynolds number (Re_x) for each of the test conditions is presented in Table 2. Seven unsteady temperature gauges were installed on the cylinder; however, only four are highlighted in this work because only four signal-conditioning amplifiers were available. Each temperature gauge provides a fast time response greater than 100 kHz and a high output sensitivity of 0.5 mV/°F, with a thermal response of 0.0045 °F/μs. The sensing element is housed in a cartridge with an outer diameter of 1.59 mm (0.0625 in), which is encased in a 316 stainless steel sleeve with a 6.36 mm (0.25 in) outer diameter to match the material and wall thickness of the HCF model. The exposed

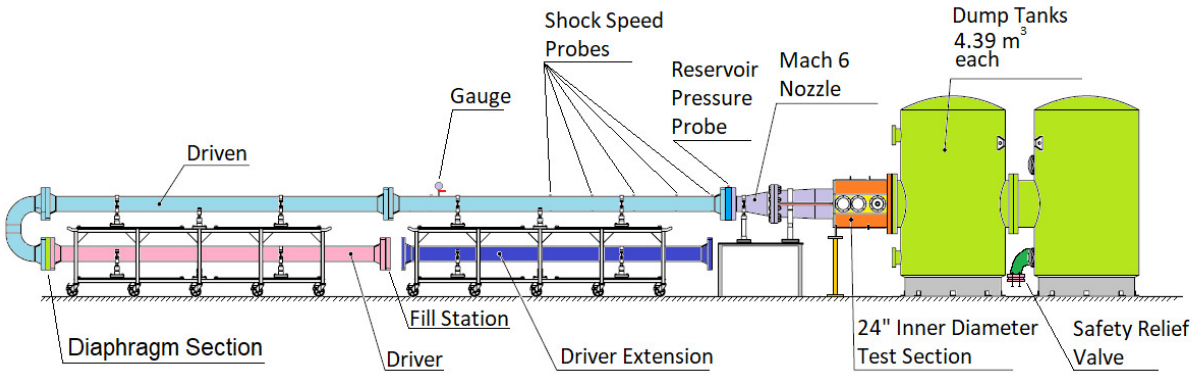

Fig. 1 Schematic of Stevens Shock Tunnel. Drawing to scale with respect to 5 m long driver tube denoted in pink.

surfaces of the gauges are contoured to align with the outer diameter of the hollow cylinder.

Table 2 Axial locations and distance from the leading edge for the unsteady temperature gauges. Local Reynolds number for both run conditions and is defined as $\rho_e U_e x/\mu_e$.

	Distance from leading edge	Re_x*10^6 'cold-flow'	Re_x*10^6 'enthalpy match'
Gauge 1	9.0	2.65	1.24
Gauge 3 (FLDI Location)	27.6	8.10	3.79
Gauge 5	31.1	9.15	4.28
Gauge (KTV Location)	33.1	9.73	4.56

Each cartridge provides two outputs: an instrumentation cable for the unsteady temperature signal and a Type-T thermocouple embedded within the housing. The instrumentation lead is routed through a facility feed-through plate and terminated at an external completion box. The completion box output is then connected to a Stanford Research SR560 constant-voltage preamplifier, configured with a 100 kHz low-pass filter and a gain of 1. The amplified signal is subsequently digitized using a PXIe-6378 data acquisition card operating at 3 MHz.

The wall shear sensors provide a measurement bandwidth from 250 Hz and higher, with the ability to resolve shear stresses as low as 25 Pa. Each sensor is housed in a 6.36 mm (0.25 in) diameter package, making it fully interchangeable with the temperature gauges on the HCF cylinder. Like the temperature sensors, the exposed surfaces of the shear sensors are contoured to match the outer diameter of the hollow cylinder. Proper orientation of each sensor is critical, as the device produces a voltage drop when the applied shear stress is directed upstream along the surface of the cylinder. The sensor output is routed to a built-in amplifier that completes the Wheatstone bridge and applies a 5 kHz low–pass filter and a gain of 1000 prior to external data acquisition. The amplified signal is digitized using a Cleverscope C328A digital oscilloscope operating at 100 MHz.

III. Results

A. Recovering heat flux from the unsteady temperature gauges

The captured temperature data were imported into MATLAB and processed as follows: (1) smoothed using a three-point moving average with MATLAB's `smooth` filter; (2) converted from volts to millivolts; (3) converted to degrees Fahrenheit using the manufacturer's sensitivity curve; (4) converted to Kelvin. A wind-off interval was identified, and the mean temperature over this period was taken as the reference temperature for the experiment. The measured temperatures were then shifted by this reference value to obtain ΔT.

Two methods were applied to recover the surface heat flux: (1) the Cook–Felderman approach and (2) an inverse FFT method based on Green's functions. The Cook–Felderman method assumes one–dimensional heat transfer in a

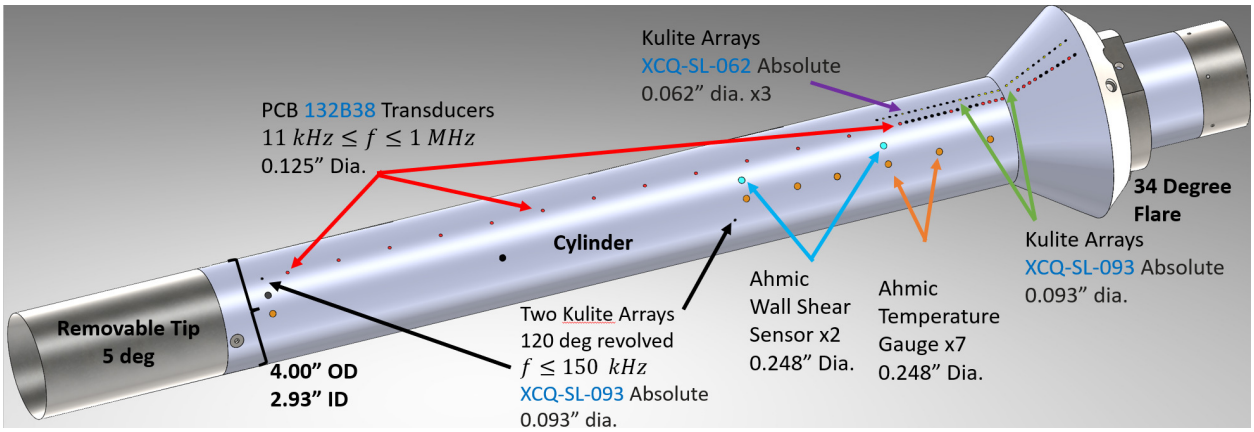

Fig. 2 Schematic of re-instrumented hollow-cylinder flare test article. Unsteady temperature gauges are denoted in orange and wall shear stress gauges are denoted in cyan.

semi-infinite medium with constant thermophysical properties. The relevant properties of the epoxy surrounding the temperature sensor are: $k = 0.572$ W/m-K, $C_p = 1197$ J/kg-K, and $\rho = 1500$ kg/m^3. The Cook–Felderman formulation used in this work is given in Eq. 1.

$$\dot{q}(t) = 2\sqrt{\frac{k\,\rho\,c}{\pi}} \sum_{i=1}^{n} \frac{T(t_i) - T(t_{i-1})}{\sqrt{t_n - t_i} + \sqrt{t_n - t_{i-1}}} \tag{1}$$

where:

$\dot{q}$ = Heat flux (W/m^2);
k = Thermal conductivity (W/mK);
ρ = Density (kg/m^3);
c_p = Specific heat capacity (J/kgK);
T_i = Temperature at time i;
t_i = Time at the end of the i^{th} time interval;
n = the total length of the time vector.

The second method used was an FFT inversions using the Green's function, as shown in Marineau and Hornung [10].

$$\dot{q}_i = \mathcal{F}^{-1}\left\{\frac{\mathcal{F}\{\Delta T_i\}}{\mathcal{F}\{g_i\}}\right\} \tag{2}$$

where the Green's function g is expressed as:

$$g(x,t;0,\tau) = \sqrt{\frac{\alpha}{\pi k^2 (t-\tau)}}\exp\left(-\frac{x^2}{4\alpha(t-\tau)}\right) \tag{3}$$

For this work, the sensor junction depth, x, is considered zero due to the blended surface. This simplifies Eq. 3 to:

$$g(x,t;0,\tau) = \sqrt{\frac{\alpha}{\pi k^2 (t-\tau)}} \tag{4}$$

Both the FFT of the temperature change and the Green's function were shifted to the center of the spectrum and filtered using a 100 kHz low–pass filter. A comparison of the recovered heat flux obtained from the two methods is presented in Fig. 3 for temperature gauge 6. For both test conditions, the Cook–Felderman results show good agreement with the inverse FFT Green's function approach, with all traces follow the same overall trend. The acquired temperature rise and recovered heat flux for the two run conditions is presented in Fig. 4. It is important to note that gauge 1 was disturbed by secondary diaphragm material, leading to unexpected behavior during the test time.

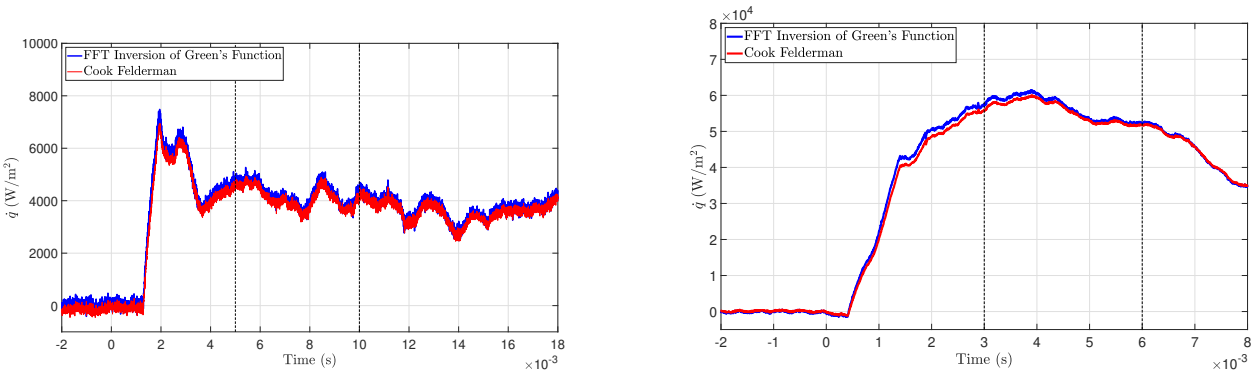

(a) Shot 518 Gauge 6 **(b) Shot 521 Gauge 6**

Fig. 3 Comparison of recovered heat flux using Cook-Felderman (red) and Green's function (blue) for temperature gauge 6. Test time for each condition is denoted with vertical dashed lines.

B. Recovering Shear Stress Using Wall Shear Sensors

The captured wall–shear data were imported into MATLAB and processed as follows: (1) converted from volts to millivolts; (2) downsampled to 5 kHz to match the hardware; (3) smoothed using a 300,000-point moving average. As done for the temperature gauges, a wind-off reference interval was identified, and the mean over this interval was subtracted from the signal to tare the data. The tared voltage signal was then multiplied by the manufacturer's sensitivity to obtain the corresponding wall shear stress.

Wall shear values for shot 521 are presented in Fig. 5. The 'enthalpy-matched' condition is the only experiment with wall shear above the noise threshold for the sensors. Although the longer test time available in the 'cold-flow', the expected shear using the Reynolds analogy from the KTV data is 23 Pa [14], which could not be resolved.

IV. Discussion

To compare the heat transfer across both run conditions and sensor locations, the dimensional wall heat flux is expressed in terms of the Stanton number,

$$St = \frac{\dot{q}}{\rho_e U_e C_p \left(T_w - T_e\right)}, \tag{5}$$

where ρ_e, U_e, and T_e are the local edge density, velocity, and temperature obtained from the facility freestream calculation, and T_w is the adiabatic wall temperature. The Reynolds analogy was used to correlate skin friction coefficient, obtained from the wall shear sensors, to Stanton number. The skin friction C_f from the wall shear stress is done using Eq. 6.

$$C_f = \frac{2\tau_w}{\rho_e U_e^2} \tag{6}$$

where τ_w is the wall shear stress obtained from the sensors. Stanton number is then determined using the Reynolds analogy presented in Eq. 7

$$St = \frac{1}{2} C_f \, Pr^{-2/3} \tag{7}$$

where Pr$\approx$ 0.75.

The experimentally obtained Stanton number and Reynolds number are correlated to both laminar and turbulent flow conditions. The laminar correlation starts with the Reynolds analogy from Eq. 7. The compressible skin friction coefficient $C_{f,\text{comp}}$ is evaluated using the reference temperature model [22]:

$$C_{f,\text{comp}}(x) \approx \frac{0.664}{\sqrt{Re_x}} \sqrt{C^*} \tag{8}$$

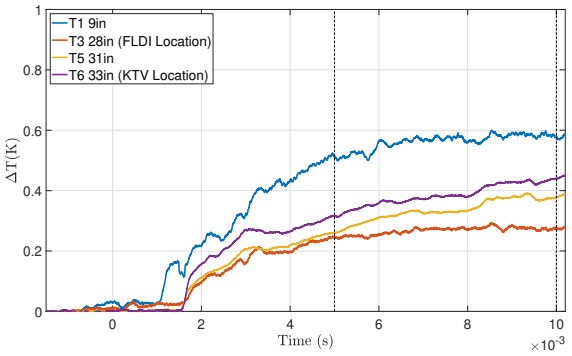

(a) Shot 518

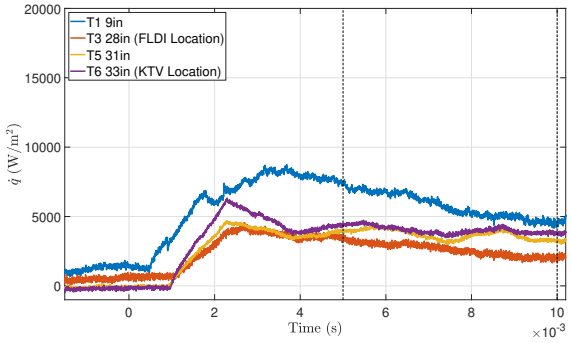

(b) Shot 518

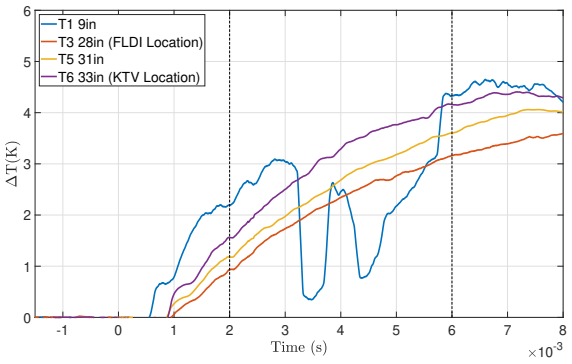

(c) Shot 521

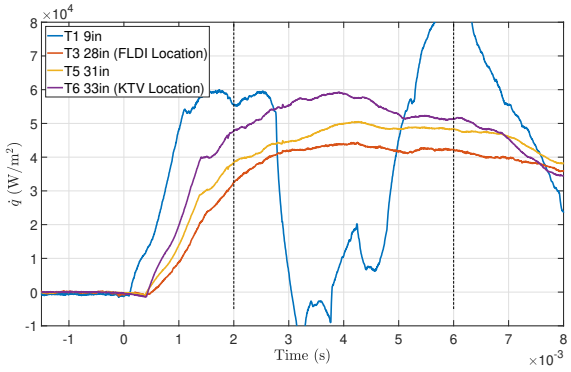

(d) Shot 521

Fig. 4 ΔT and $\dot{q}$ for Shot 518 and 521. Steady test time is denoted by dashed vertical lines.

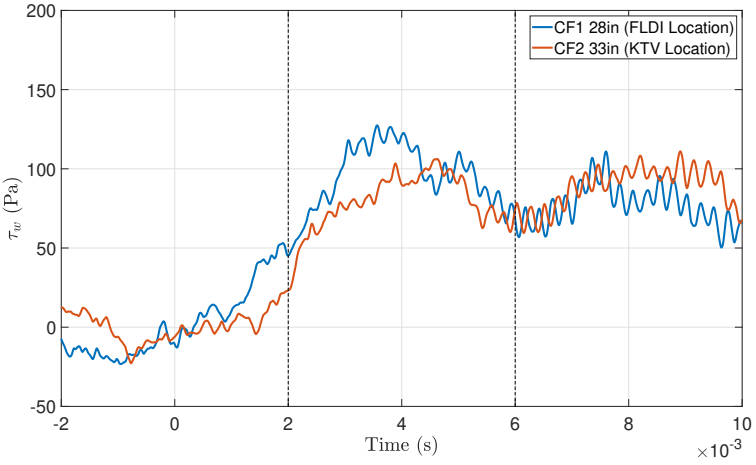

Fig. 5 Measured wall shear stress for Shot 521. Steady test time is denoted by dashed vertical lines.

where $C^* = \rho^*\mu^*/\rho_e\mu_e$ and the reference temperature T^* is determined by:

$$\frac{T^*}{T_e} = \frac{1}{2} + \frac{\gamma - 1}{2}\frac{\sqrt{Pr}}{6}M_e^2 + \frac{1}{2}\frac{T_w}{T_e} \tag{9}$$

The turbulent correlation starts again with the Reynolds analogy. For a flat plate, White [2] defines the incompressible skin friction as:

$$C_{f,\text{inc}} \approx \frac{0.455}{\ln^2(0.06\,Re_x)} \tag{10}$$

White [2] presented a calculation, seen in Eq. 11 to relate incompressible skin friction to compressible skin friction over a flat plate by means of a transformation factor:

$$C_{f,\text{comp}} = \frac{1}{F_c}\,C_{f,\text{inc}}(Re_x F_{Re}) \approx \frac{1}{F_c}\frac{0.455}{\ln^2(0.06\,Re_x F_{Re})} \tag{11}$$

where F_c is the skin friction correlation factor:

$$F_c = \frac{Tr/T_\infty - 1}{(sin^{-1}A + sin^{-1}B)^2} \tag{12}$$

F_{Re} is the "stretching factor" proposed by White and Christoph [23]:

$$F_{Re} = \frac{1}{\sqrt{F_c}}\frac{\mu_e}{\mu_w}\sqrt{\frac{T_e}{T_w}} \tag{13}$$

and

$$\begin{aligned} A &= \frac{2a^2 - b}{\left(b^2 + 4a^2\right)^{1/2}}, \quad B = \frac{b}{\left(b^2 + 4a^2\right)^{1/2}}, \\ a &= \left(r\frac{\gamma - 1}{2}M_\infty^2\frac{T_\infty}{T_w}\right)^{1/2}, \quad b = \frac{T_r}{T_w} - 1. \end{aligned} \tag{14}$$

The results from both Shot 518 and 520 are compared to correlations for the laminar and turbulent flow conditions in Fig.6. For Shot 518 in Fig. 6a, the Stanton number acquired using krypton tagging velocimetry (KTV) during a previous campaign [14] is plotted. The KTV tagging is at the same axial location downstream of the leading edge as gauge 6. For shot 521 in Fig.6b, Stanton number resolved from wall shear measurements are also plotted. Wall shear sensor 1 and 2 are at the same axial location as temperature gauge 3 and 6. Additionally, it is important to note that the evaluated test time for gauge 1 is adjusted to be 2 ms to 2.5 ms due to the disturbance after this time.

Based on the correlations, the temperature gauges' measured Stanton number undershoots by about 50%. The authors are still examining the experimental causes to explain this error. Since both of the experiments yield values that undershoot the same amount, the error seems to be hardware related over processing or run condition based. The wall shear sensors yield reasonable Stanton numbers, although slightly lower than expected. The SNR for these sensors are low and therefore the data is smoothed to the limitation of the experiment. The smoothing may have slightly dampened the signal, resulting in the lower Stanton number since Stanton and C_f are linearly related.

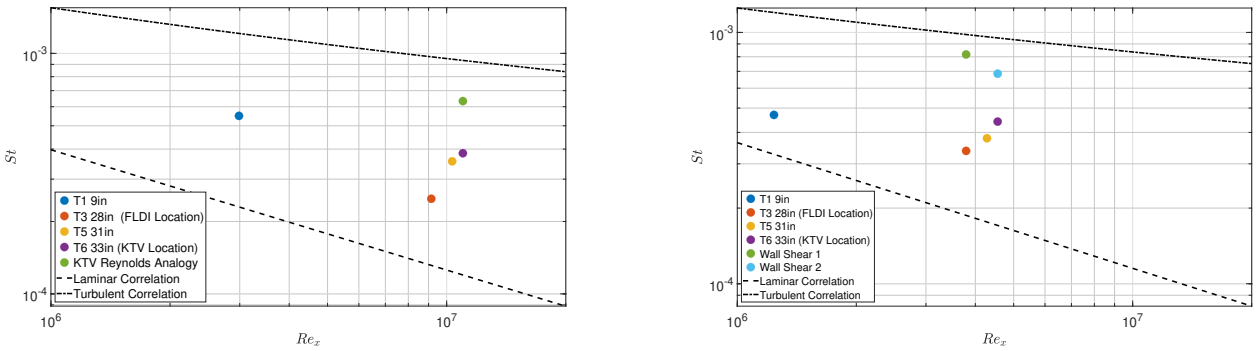

(a) **(b)**

Fig. 6 Time-averaged plot of non-dimensional heat transfer results in terms of Stanton number vs. Reynolds number for (a) Shot 518 and (b) Shot 521. Laminar and turbulent correlations are presented. Also presented is the Stanton Number from the KTV in (a) and the wall shear correlated Stanton number in (b).

V. Error in Heat-Transfer Analysis

The heat-transfer results in the previous sections are consistently lower than expected, per the correlations. One explanation for this is the finite depth of the sensing element. Following Schultz and Jones [4] Eq. 35,

$$\frac{\dot{q}_{measured}}{\dot{q}_{actual}} = 1 - \frac{L}{\sqrt{\pi t \alpha_s}}\left(\frac{1}{a} - \frac{a}{2}\right), \tag{15}$$

where $a = \sqrt{\rho_e c_{pe} k_e / (\rho_s c_{ps} k_s)}$ and L is the sensing element depth. The density, thermal conductivity, specific heat, and diffusivity are ρ, c_p, k, and α, respectively with e and s subscripts representing the epoxy and silicon sensing element, respectively. The error from Eq. 35 and an estimate of what the expected results should be is included in Fig. 7. Also included in the figure is a revised heat-transfer estimate from Whalen et al. [1] which accounts for finite sensor depth. The revised Whalen et al. [1] calculations match reasonably well with the correction to the Cook-Felderman method. This brings confidence to the heat-flux measurements once the finite sensor depth is accounted for. The effect is rather large, especially at early test times. Correcting all the previous heat-transfer calculations will be performed as future work. Equation 35 from Schultz and Jones [4] cannot be applied as it is here in a strict sense because the heat flux is transient and initialized at a different time. It is meant to serve as a notional value.

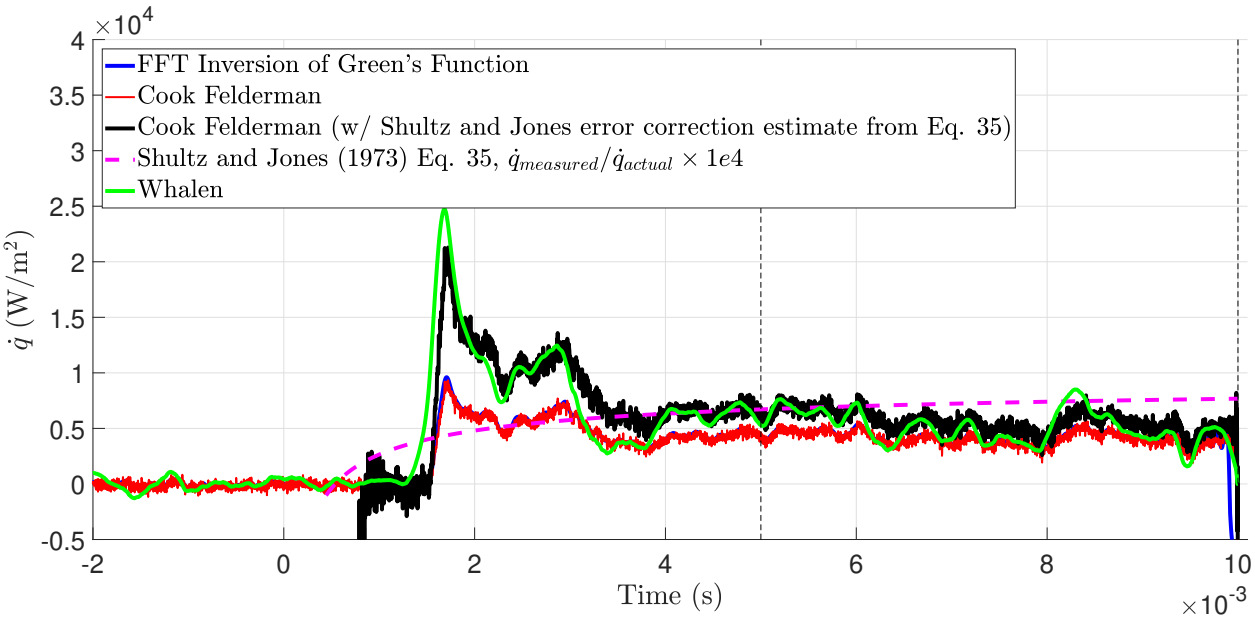

Fig. 7 Heat flux vs time for Shot 518. The FFT and Cook-Felderman methods were used. Eq. 35 from Schultz and Jones [4] is shown, showing errors from 40-60% due to finite sensor depth. Finally, the method of Whalen et al. [1] shows good agreement with the Cook-Felderman results once the approximate correction is made to account for sensor depth.

VI. Conclusion and Future Work

Ahmic aerospace unsteady temperature gauges and wall shear sensors were instrumented to a hollow-cylinder flare test article in the Stevens Shock Tunnel. Two experimental run conditions were performed: an 'enthalpy-matched' condition which replicates free-flight Mach 6 conditions at 20 km for ≈ 5 ms, and a 'cold flow' condition which has longer test time of ≈ 15 ms and larger Reynolds numbers. The temperature gauges deemed sensitive enough to capture the flow dynamics in the short timescales including shock arrival and noisy test start up to quieter steady test time. Non-dimensionalising the recovered heat flux to Stanton Number vs Reynolds number shows 50% undershoot to the value theorized by correlations for turbulent flow conditions. In the future, the method of Whalen et al. [1] will be used to correct for errors associated with the sensing element being of finite depth.

The wall shear sensors were capable of resolving measurements at small timescales but were unable to capture dynamics at low shear conditions ($\tau < 50$ Pa). The Stanton number evaluated by using the Reynolds analogy with the

measured data resulted in reasonable agreement with the turbulent correlation.

Acknowledgments

Ben A. Segall, Tim C. Keenoy, and Nicholaus J. Pariale were supported by ONR Grants, including N00014-20-1-2682, N00014-20-1-2637, N00014-23-1-2474. We thank Eric Marineau and the Office of Naval Research for sponsoring the construction and development of the Stevens Shock Tunnel. We also thank Ahsan Hameed, Jett Langhorn, Jaden Kokinakos, Ryan Ward, and Thomas Wohlbruck for their assistance in running the Stevens Shock Tunnel.

References

[1] Whalen, T. J., Laurence, S. J., Marineau, E. C., and Ozawa, H., "A Green's function approach to heat-flux estimation from temperature-sensitive paint measurements," *Measurement Science and Technology*, Vol. 32, No. 11, 2021, p. 114011. https://doi.org/10.1088/1361-6501/ac16ee.

[2] White, F., *Viscous Fluid Flow*, 2nd ed., McGraw-Hill, 1991.

[3] Leyva, I. A., "The relentless pursuit of hypersonic flight," *Physics Today*, Vol. 70, No. 11, 2017, pp. 30–36. https://doi.org/10.1063/PT.3.3762.

[4] Schultz, D. L., and Jones, T. V., "Heat-Transfer Measurements in Short-Duration Hypersonic Facilities," AD0758590, 1973.

[5] Kurits, I., Lewis, M. J., Hamner, M. P., and Norris, J. D., "Development of a Global Heat Transfer Measurement System at AEDC Hypervelocity Wind Tunnel 9," *2007 22nd International Congress on Instrumentation in Aerospace Simulation Facilities*, IEEE, Pacific Grove, CA, 2007. https://doi.org/10.1109/ICIASF.2007.4380905.

[6] Bitter, M., Hilfer, M., Schubert, T., Klein, C., and Niehuis, R., "An Ultra-Fast TSP on a CNT Heating Layer for Unsteady Temperature and Heat Flux Measurements in Subsonic Flows," *Sensors*, Vol. 22, No. 2, 2022, p. 657. https://doi.org/10.3390/s22020657.

[7] Sunyoung, L., Vergeer, L., Marin, J., Gross, A., Shu, F., and Frankel, J., "Analysis of Fast Thin Film Temperature Gauges for Hypersonic Environments," *AIAA SCITECH 2025 Forum*, AIAA, Orlando, FL, 2025. https://doi.org/10.2514/6.2025-2843.

[8] Holden, M. S., Wadhams, T. P., and MacLean, M. G., "Measurements in Regions of Shock Wave/Turbulent Boundary Layer Interaction from Mach 4 to 10 at Flight Duplicated Velocities to Evaluate and Improve the Models of Turbulence in CFD Codes," Tech. rep., CUBRC, 2014.

[9] Holden, M. S., Carr, Z. R., Wadhams, T. P., and MacLean, M. G., "Measurements in Regions of Shock Wave/Turbulent Boundary Layer Interaction from Mach 4 to 7 at Flight Duplicated Velocities to Evaluate and Improve the Models of Turbulence in CFD Codes," *2018 AIAA Aviation*, Atlanta, GA, 2018, p. 3706.

[10] Marineau, E. C., and Hornung, H. G., "Modeling and calibration of fast-response coaxial heat flux gages," *Proceedings of 47th AIAA Aerospace Sciences Meeting Including the New Horizons Forum and Aerospace Exposition*, Orlando, Florida, 2009. https://doi.org/10.2514/6.2009-737.

[11] Zhang, S., Wang, Q., Li, J., Zhang, X., and Chen, H., "Coaxial Thermocouples for Heat Transfer Measurements in Long-Duration High Enthalpy Flows," *Sensors*, Vol. 20, No. 18, 2020, p. 5254. https://doi.org/10.3390/s20185254.

[12] Meritt, R., Schetz, J., Marineau, E., and Lewis, D., "Direct Measurements of Skin Friction at AEDC Hypervelocity Wind Tunnel 9," *53rd AIAA Aerospace Sciences Meeting*, AIAA, Kissimmee, Florida, 2015. https://doi.org/10.2514/6.2015-1914.

[13] Molinaro, N. J., and Meritt, R., "Skin Friction Sensor Measurement Uncertainty," *AIAA Scitech 2019 Forum*, AIAA, San Diego, California, 2019.

[14] Segall, B. A., Keenoy, T. C., Kokinakos, J. C., Langhorn, J. D., Hameed, A., Shekhtman, D., and Parziale, N. J., "Hypersonic turbulent quantities in support of Morkovin's hypothesis," *Nature Communications*, Vol. 16, No. 9584, 2025. https://doi.org/10.1038/s41467-025-65398-4.

[15] Shekhtman, D., Hameed, A., Segall, B. A., Dworzanczyk, A. R., and Parziale, N. J., "Initial Shakedown Testing of the Stevens Shock Tunnel," *Proceedings of AIAA SciTech 2022*, AIAA 2022-1402, San Diego, California and Virtual Event, 2022. https://doi.org/10.2514/6.2022-1402.

[16] Segall, B. A., Shekhtman, D., Hameed, A., Chen, J. H., and Parziale, N. J., "Profiles of streamwise velocity and fluctuations in a hypersonic turbulent boundary layer using acetone tagging velocimetry," *Experiments in Fluids*, Vol. 64, No. 122, 2023. https://doi.org/10.1007/s00348-023-03647-2.

[17] Segall, B. A., Shekhtman, D., Langhorn, J., and Parziale, N. J., "Improved Debris Blocker and Flow Terminator in a Shock Tunnel," *Proceedings of AIAA Scitech 2024*, AIAA 2024-2570, Orlando, Florida, 2024. https://doi.org/10.2514/6.2024-2570.

[18] Goodwin, D. G., Moffat, H. K., Schoegl, I., Speth, R. L., and Weber, B. W., "Cantera: An Object-oriented Software Toolkit for Chemical Kinetics, Thermodynamics, and Transport Processes," *https://www.cantera.org*, 2022. https://doi.org/10.5281/zenodo.6387882.

[19] Browne, S. T., Ziegler, J. L., Bitter, N. P., Schmidt, B. E., Lawson, J., and Shepherd, J. E., "Numerical Solution Methods for Shock and Detonation Jump Conditions," GALCIT - FM2018-001, Caltech, 2018.

[20] Korte, J. J., Lafferty, J. F., Smith, M. S., Lewis, D. R., Butcher, C. W., Fredrick, N. J., Zarzecki, M., and Tatum, K. E., "Determination of Hypervelocity Freestream Conditions for a Vibrationally Frozen Nitrogen Flow," *Proceedings of AIAA SciTech 2021*, AIAA-2021-0981, Virtual Event, 2021. https://doi.org/10.2514/6.2021-0981.

[21] Chen, J. H., Hameed, A., Parziale, N. J., Roy, D., and Duan, L., "Spectral Analysis of Mach 6 Turbulent Boundary Layer over a Hollow Cylinder with FLDI and DNS," *Proceedings of AIAA Scitech 2024*, AIAA 2024-2734, Orlando, Florida, 2024. https://doi.org/10.2514/6.2024-2734.

[22] Dorrance, W. H., *Viscous Hypersonic Flow*, McGraw-Hill, 1962.

[23] White, F. M., and Christoph, G. H., "A Simple Theory for the Two-Dimensional Compressible Turbulent Boundary Layer," *Journal of Basic Engineering*, Vol. 94, No. 3, 1972, pp. 636–642. https://doi.org/10.1115/1.3425519.